

COVER PAGE

Document downloaded by @DAEL

Sun Nov 29 08:17:55 2026
For personal use

When automatic English translation is provided, only the original document is authentic.
The EAA cannot be held responsible of any translation error

Bibliographical reference

On the Use of Linear Acoustic Multiports to Predict Whistling in Confined Flows, Mikael Karlsson and Mats Åbom, Acta Acustica **vol. 97** (Number 1), 2011, pp. 24-33

DOI
https://doi.org/10.3813/AAA.918383

Acta Acustica united with Acustica
Vol. 97 (2011) 24 – 33

DOI 10.3813/AAA.918383

On the Use of Linear Acoustic Multiports to Predict Whistling in Confined Flows

Mikael Karlsson[1], Mats Åbom[2]

[1] KTH Cicero, The Marcus Wallenberg Laboratory for Sound and Vibration Research, Teknikringen 8, 100 44 Stockholm, Sweden. kmk@kth.se

[2] KTH, Linné Flow Centre Teknikringen 8, 100 44 Stockholm, Sweden. matsabom@kth.se

Summary

The use of linear acoustic multiport models to analyse the existence of flow driven instabilities, that is – self-sustained oscillators or whistles – is addressed. By combining the scattering and reflection matrices for a system and searching for eigenfrequencies (zeros) in the critical half-plane, the existence of exponentially growing instabilities can be determined. In practice, the available frequency domain data are only known along the real axis; then the search for zeros may be done via the so-called Nyquist stability criterion generalized to an N-degree of freedom system. The method has been validated by two test cases, a T-junction and a Herschel-Quincke tube. In both cases, the occurrence and the frequencies of the self-sustained oscillations were correctly predicted.

PACS no. 43.28.Py

1. Introduction

Complex flow duct networks such as gas transport systems, ventilation systems and vehicle intake and exhaust systems offer a significant challenge to anyone involved in aeroacoustic modelling. A common simplification is to reduce the system under study to a network of linear acoustic multiports [1]. For simple geometries, the passive or acoustic scattering properties of a multiport can be determined analytically, but for more complicated geometries, numerical or experimental methods have to be used. Reduced to the low frequency plane wave range, the multiport (often limited to one and two ports) methodology is well established and is used in industry for studying sound transmission and reflection. The use of the full multiport model, including the active (source) part, has been demonstrated, for example, with IC-engine intake and exhaust noise and fans [2].

Of recent interest is the application of multiport models to sound generation and flow-acoustic coupling in ducts associated with flow separation [3, 4]. One interesting question is whether it is possible to predict sound amplification using linear models. Amplification at a certain frequency could then result in self-sustained oscillations ("whistling"), provided the appropriate reflecting boundaries are present. The use of linear multiport models to study thermo-acoustic instabilities [5, 6] is a related problem.

Although self-sustained oscillation is a nonlinear process, it has been argued that the occurrence and frequency of such phenomena may be studied using linear stability analysis [7]. Linear stability analysis applied to multiport networks is common in applied control theory – for example, in the design of microwave or radio frequency circuits. The methods used include S-matrix stability [8, 9] and Nyquist stability [10]. The latter is basically an implementation of the argument principle from complex analysis, which is used to find the number of poles and zeros of a frequency domain function. Normally Nyquist stability is defined using the Laplace transform. However, assuming a complex angular frequency, it is equivalent to use the Fourier transform. Since the Fourier transform is the more common choice in acoustics, it is used here. Assuming the temporal Fourier transform is defined using $\exp(-\mathrm{i}\omega t)$, the domain where zeroes and poles are sought is the lower half-plane ($\Im m(\omega) < 0$).

Fletcher and Rossing [11] and Howe [7], for example, have applied a more limited approach to flow-acoustic coupling than the general multiport formulation, which is also based on the study of stability by identifying poles or zeros in the critical half-plane. This approach is applicable when the flow- acoustic coupling can be reduced to a single impedance ("Rayleigh impedance" in Howe's notation). For the total system to become unstable, the Rayleigh impedance must overcome internal losses and the radiation impedance. Frequencies where the system can become unstable are then identified as close to the real part $\Re e(\omega)$ of the zeros of the total impedance,

$$Z = Z_R + Z_{ac}, \tag{1}$$

where Z_R is the Rayleigh impedance and Z_{ac} represents the acoustic system it is coupled to. If one can determine the complex zero, one can also estimate the growth rate of

Received 16 May 2010,
accepted 20 September 2010.

© S. Hirzel Verlag · EAA

the instability that will be proportional to $\exp[|\Im m(\omega)|t]$. The actual amplitude of the self-sustained oscillations, which is determined by the saturation given by nonlinear effects [7], cannot, of course, be determined.

In this work, the flow-acoustic interaction effects – in the form of aperture tones – are studied following the multiport formalism. First, the theory of the inclusion of these phenomena in the linear multiport and the means for quantifying the amplification or attenuation are given. This only indicates the potential for a fluid-driven whistle or the frequency regions where amplification exists. To close the problem, the systems acoustic response ("feedback") with a given termination is derived. Stability analysis can then be applied as a simple eigenvalue problem for the complete system. Second, the formalism is validated experimentally in two configurations based on T-junctions. First by a single T-junction with a resonator arrangement and then by two interacting T-junctions.

2. Theory

An active acoustic multiport is a linear and time invariant black box with N degrees of freedom, which in the frequency domain can be written as [2]:

$$\hat{\boldsymbol{x}}_+ = \boldsymbol{S}\hat{\boldsymbol{x}}_- + \hat{\boldsymbol{x}}^{s+}, \tag{2}$$

where $\hat{\boldsymbol{x}}$ is the state variable of choice, and the plus and minus signs indicate travelling wave amplitudes out of (+) and into (−) the multiport. Consequently, the passive properties of the system, the reflection and transmission of sound, are represented by the scattering matrix $\boldsymbol{S}$. The vector $\hat{\boldsymbol{x}}^{s+}$ represents sources within the system that normally are assumed to be independent of the sound field; this is often a good assumption when modelling fluid machines [12]. However, for flow-generated sound, the interaction of the hydrodynamic and acoustic fields should be included. This can be done by allowing the unsteady flow associated with the sound generation to be modulated by the incident acoustic waves. The source strength vector $\hat{\boldsymbol{x}}^{s+}$ is then split into two parts, one corresponding to the modulation given by the incident acoustic field while the other represents the part that is independent of the acoustic field. The modulated part can be expressed as

$$\hat{\boldsymbol{x}}^{s+}_{\text{mod}} = \boldsymbol{S}_m\hat{\boldsymbol{x}}_-, \tag{3}$$

that when inserted into equation (2) yields

$$\hat{\boldsymbol{x}}_+ = \big(\boldsymbol{S}_0 + \boldsymbol{S}_m\big)\hat{\boldsymbol{x}}_- + \hat{\boldsymbol{x}}_0^{s+}, \tag{4}$$

where the subscript zero indicates the original scattering matrix and source vector – that is, those variables independent of the source coupling. Hence, a linear modulation of the source term simply adds to the scattering properties. This in turn implies that in an experimental characterisation of a multiport, any information on flow-acoustic interaction effects is included in the scattering matrix representation, while the resulting source vector is always independent of the incident acoustic field. For the flow separation type of configuration studied here (T-Junction), the flow-acoustic interaction effect can be described as a vortex-sound mechanism [7].

2.1. Whistling potentiality

Now assuming that the flow-acoustic interaction effects are included in the linear scattering matrix $\boldsymbol{S} = \boldsymbol{S}_0 + \boldsymbol{S}_m$, the potential for a system to whistle can be examined by computing a power balance over the multiport. Here it is useful to adopt an alternative state variable [13] that is simply related to the time-averaged power as $\langle P_\pm\rangle = \hat{x}^*_\pm\hat{x}_\pm$. Now, denoting the scattering matrix in the new variable $\boldsymbol{S}_p$, the time-averaged acoustic power for a given incident acoustic field is

$$\big\langle P_{\text{out}}\big\rangle = \hat{\boldsymbol{x}}^*_-\big(\boldsymbol{S}^*_P\boldsymbol{S}_P\big)\hat{\boldsymbol{x}}_- - \hat{\boldsymbol{x}}^*_-\hat{\boldsymbol{x}}_-, \tag{5}$$

where * is the Hermitian transpose. If the flow-acoustic interaction results in an amplification of the incident sound, this equation is positive.

One use of this result is to assume excitation at only one port n at a time [4]. Although a multiport in practise is likely to experience incident sound at more than one port at a time, this approach may provide some valuable insights into the system's characteristics. Normalizing the incident power at the port of interest to unity (that is, $\hat{\boldsymbol{x}}^*_{n-}\hat{\boldsymbol{x}}_{n-} = 1$) this can be expressed as

$$\big\langle P_{\text{out}}\big\rangle = \hat{\boldsymbol{x}}^*_{n-}\big(\boldsymbol{S}^*_P\boldsymbol{S}_P\big)\hat{\boldsymbol{x}}_{n-} - 1. \tag{6}$$

A more generic approach was proposed by Aurégan and Starobinski [13]. Assuming an arbitrary excitation at all nodes with a total incident power of unity, one obtains

$$\big\langle P_{\text{out}}\big\rangle = \hat{\boldsymbol{x}}^*_-\big(\boldsymbol{S}^*_P\boldsymbol{S}_P\big)\hat{\boldsymbol{x}}_- - 1. \tag{7}$$

The quadratic form in equation (7) is Hermitian and positive definite. Thus it can be transformed into a diagonal form,

$$\hat{\boldsymbol{x}}^*_-\big(\boldsymbol{S}^*_P\boldsymbol{S}_P\big)\hat{\boldsymbol{x}}_- = \sum \lambda_n|x'_n|^2, \tag{8}$$

where λ_n are the real and positive eigenvalues of $(\boldsymbol{S}^*_P\boldsymbol{S}_P)$ and the vector $\boldsymbol{x}'_-$ is given by $\boldsymbol{x}_- = \boldsymbol{T}\boldsymbol{x}'_-$. The transformation matrix $\boldsymbol{T}$ is a unitary matrix where the columns represent the eigenvectors of the Hermitian matrix $(\boldsymbol{S}^*_P\boldsymbol{S}_P)$. Finally, inserting equation (8) into equation (7), the maximum (or minimum) time-averaged acoustic power output can be expressed as

$$\big\langle P_{\max}\big\rangle = \lambda_{\max} - 1, \tag{9}$$

$$\big\langle P_{\min}\big\rangle = \lambda_{\min} - 1. \tag{10}$$

That is, an eigenvalue larger than unity indicates amplification of the incoming perturbation. These last results include all possible excitation combinations. The actual relative excitation yielding a maximum (or minimum) can be found by studying the corresponding eigenvector.

2.2. Response with a given termination

The power balances described in the previous section indicate the Strouhal number ranges at which the given multiport amplifies or attenuates incident acoustic waves. The actual response to a given termination can be studied by introducing a reflection matrix $\boldsymbol{R}$ whose elements represent the passive and time invariant terminations of the system seen at each port.

$$\hat{\boldsymbol{x}}_- = \boldsymbol{R}\hat{\boldsymbol{x}}_+. \tag{11}$$

Inserting this into equation (2) yields

$$\hat{\boldsymbol{x}}_+ = \boldsymbol{S}\boldsymbol{R}\hat{\boldsymbol{x}}_+ + \hat{\boldsymbol{x}}^{s+}. \tag{12}$$

The source vector is independent of the passive part of the multiport. Hence, eigenvalues of the system representing growing modes can be found studying,

$$\big(\boldsymbol{E} - \boldsymbol{S}\boldsymbol{R}\big)\hat{\boldsymbol{x}}_+, \tag{13}$$

where $\boldsymbol{E}$ is the unit matrix. This equation has non-trivial solutions (eigenfrequencies) when

$$D = \det\big(\boldsymbol{E} - \boldsymbol{S}\boldsymbol{R}\big) = 0. \tag{14}$$

If the system is reflection free ($\boldsymbol{R} \equiv 0$), the function D collapses to a single point $(1, \mathrm{i}0)$ in the complex $D(\omega)$-plane.

2.3. Linear stability

There are various methods for finding the zeros of the complex function $D(\omega)$. One method is to apply Cauchy's principle of the argument for complex functions. Assume that $D(\omega)$ is analytical (except at a finite number of points) in the complex plane ω. Now, travelling around a closed contour (at which $D(\omega)$ must be analytical) in a clockwise direction, $D(\omega)$ encircles the origin in the complex $D(\omega)$ plane in the same direction N times, where N is given by

$$N = Z - P, \tag{15}$$

where Z and P stand for the zeros and poles of the function $D(\omega)$ inside the contour. If there are no poles in D, then N represents the number of zeros. Assuming that the system under study is causal and that the acoustic reflections tend to zero for large ω implies that it is sufficient to study the variation of $D(\omega)$ along the real axis only. For large ω, $D(\omega)$ approaches the same point $(1, \mathrm{i}0)$ in the lower half-plane as for large ω along the real axis. Hence, closing the contour in the lower half-plane is not necessary since for large ω this simply corresponds to the point $(1, \mathrm{i}0)$ already included. Also, since roots and poles appear in pairs (i.e., for each root/pole with a positive real part there is a corresponding part located at $-\omega^*$) it is sufficient to investigate only the positive real axis. This creates a clockwise contour covering the critical lower half-plane where zeros represent exponentially growing eigenfrequencies. This version of the argument principle can be seen as an extension of the so-called Nyquist stability criterion to an N-DOF system. Like the traditional Nyquist criterion, an estimate of the eigenfrequencies (the real part) is found when the function $D(\omega)$ crosses the negative real axis, thus completing one encirclement [6, 14]. The distance to zero at this crossing can be seen as a measure of the growth rate of the instability.

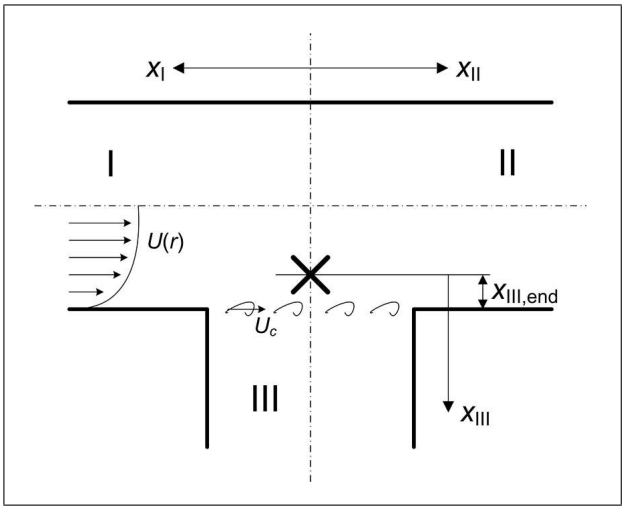

Figure 1. T-junction definition with coordinates. r is the radial distance from the centreline.

The requirement that there are no poles in D in the lower plane implies that $\boldsymbol{S}$ and $\boldsymbol{R}$ must have no poles. Physically, this implies that the equations $\boldsymbol{S}^{-1}\hat{\boldsymbol{x}}_+ = 0$ and $\boldsymbol{R}^{-1}\hat{\boldsymbol{x}}_- = 0$ have no zeros in the lower half-plane; that is, neither the multiport nor the termination whistle by themselves. For the test cases studied here (with terminations consisting of dissipative silencers with reflection coefficients smaller than unity), it is sufficient to check $\boldsymbol{S}$ since there are no poles in $\boldsymbol{R}$.

An alternative to the Nyquist criterion for finding critical zeros is to perform a full system identification in order to identify all zeros and poles of $D(\omega)$. See, for example, [15]. However, for complex pipe systems there can be a large number of zeros corresponding to the duct eigenfrequencies, although normally only a few are critical. Therefore, if the purpose of the study is to analyse the stability and risk of whistling, the Nyquist criterion is a fast and efficient tool. Like the system identification approach, the Nyquist criterion can be used to study stability limits – that is, how the occurrence of an unstable zero depends on different design parameters such as the reflection coefficient at a specified port.

3. Test cases

The basis for the test cases used in this work is a T-junction that can be represented as an acoustic three-port. The T-junction is built as a straight cylindrical main duct of diameter $d = 0.057$ m to which another straight duct of the same diameter is attached perpendicularly with sharp edges, as sketched in Figure 1. The three-port is assumed acoustically compact and is collapsed to a single point denoted

with a bold X in Figure 1. This point is chosen along the centreline of the side branch at a distance into the main duct corresponding to the end correction at no flow conditions [16, 17].

The mean flow is restricted to the main duct. Thus the side branch orifice (Branch III) is subjected to grazing flow. This is a well-known case for which self-sustained oscillations can be triggered. Hydrodynamic instabilities in the shear layer interact with the acoustic field when they are convected across the orifice. Since the interaction between the hydrodynamic and the acoustic fields depends on the convection velocity of the vorticity U_c, the variation of which can be neglected for small amplitude acoustic oscillations, it is sufficient to study the linear system [18]. The interaction can be constructive or deconstructive – that is, it may either amplify or attenuate the incident sound. The actual degree of interaction depends on the incidence of the acoustic disturbance. Incident sound from the upstream duct or the side branch triggers the flow-acoustic interaction while downstream excitation yields a much weaker response [19, 4].

The dependence on the incidence of the acoustic waves is one of the driving factors for using the stability analysis as derived in equation (14) where this effect is already included. Reducing the problem to a single "Rayleigh" impedance as described, e.g., by Howe [7], is not possible for the three-port case studied here.

If the ratio $V = |u'|/U_0$ of the amplitude of the acoustic particle velocity in the orifice to the mean flow velocity is sufficiently high, the response can become nonlinear, and the shear layer disturbances tend to roll up into discrete vortices. The critical value of V for the onset of nonlinearities varies with the flow conditions, such as the boundary layer thickness, but it is typically in the order of 10^{-2} [20, 19]. Keeping the ratio of the amplitude of the particle velocity to the mean flow below the critical level, the amplification is linear and the proposed model in equation (4) holds. That is, flow-acoustic interaction effects are included in the linear scattering matrix.

First the T-junctions are characterised – that is, the scattering matrix $\boldsymbol{S} = \boldsymbol{S}_0 + \boldsymbol{S}_m$ is determined. Based on Figure 1, the following convention is used to denote the elements of the S-matrix,

$$\boldsymbol{S} = \begin{pmatrix} S_{I-I} & S_{I-II} & S_{I-III} \\ S_{II-I} & S_{II-II} & S_{II-III} \\ S_{III-I} & S_{III-II} & S_{III-III} \end{pmatrix}. \qquad (16)$$

In the determination of $\boldsymbol{S}$, care has to be taken to ensure that the system is linear. As described in the experimental section, this is done by reducing the reflections due to the system terminations. Once the scattering matrix is obtained, the power balance procedure suggested by equation (6) identifies where the system can become unstable provided there is adequate feedback.

Two systems that may provide the required feedback are tested. The first arrangement is a simple modification to the test setup for the determination of the scattering matrix. A quarter wave resonator tuned to the centre frequency of one of the identified amplification regions is placed half a wave length (of the same frequency) into the straight duct attached to the side branch (Branch III). This provides a resonant system with an acoustic particle velocity maximum at the orifice, which enhances the acoustic feedback to the vortex-sound mechanism. Results are shown for this resonator arrangement tuned towards two different amplification regions. The test for stability according to equation (14) is easily performed. The elements in the reflection matrix $\boldsymbol{R}$ are obtained from a model of the resonator combined with measured data for the reflection from the test rig terminations.

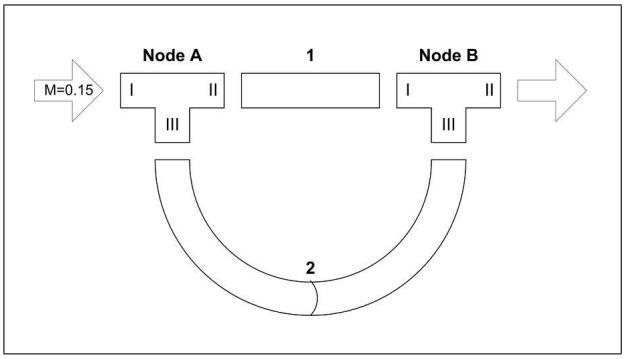

Figure 2. Herschel-Quincke test setup.

Second, to provide a more complex system, which could sustain an oscillation by internal reflections, two T-junctions are combined into a Herschel-Quincke tube [21, 22], as sketched in Figure 2. The Herschel-Quincke tube, in its classic configuration, is the parallel connection of two ducts of different lengths between two nodes. Here the T-junctions act as the nodes and the connecting ducts (1 and 2) are made of the same diameter pipe as the T-junctions. This configuration should be able to whistle due to internal reflections, that is, assuming the up- and downstream terminations are anechoic. To ensure grazing flow over the two orifices, a thin plastic film was inserted in duct two. This film blocks the mean flow in duct two but is sufficiently light that it has a negligible effect on the acoustics. This was validated by determining the scattering properties of the plastic film and including it in the stability analysis of the system. Since the effect of the introduction of the film did not affect the results, it is not included in the presentation below.

The attenuation maxima of a Herschel-Quincke tube, which can be seen as representing internal resonances, are given by two separate conditions [23]. The first condition is sensitive to differences in mean flow between the ducts and is cancelled in this case. The second condition, which in the simpler case of no mean flow stipulates the odd integral multiple of half a wave length difference predicted already by Herschel [21], is still valid with mean flow and have two interesting characteristics for this application. First, at the attenuation maxima the acoustic pressure is zero at the nodes. Second, with mean flow one obtains attenuation maxima not only at odd multiples but also at even multiples of half a wave length difference between

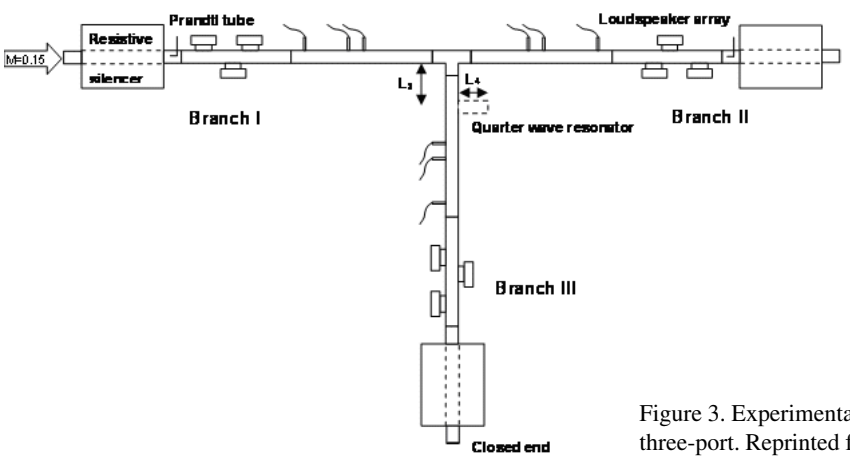

Figure 3. Experimental setup for characterisation of the active three-port. Reprinted from [4], with permission from Elsevier.

the ducts. However, as demonstrated in [23], the attenuation maxima at the even multiples are reduced when there is a difference in the mean flow between ducts one and two, while the odd multiples are less affected. The idea is now to use the pressure minima associated with the attenuation maxima in the Herschel-Quincke system in which the design counteracts the acoustic feedback needed to sustain a self-sustained oscillation. For this purpose, two configurations were tested. In one configuration, the longer of the ducts is twice the length of the shorter L_1. In the second configuration, the length ratio is three times. With the appropriate choice of L_1, this provides one system that whistles ($L_2/L_1 = 3$) and one that does not ($L_2/L_1 = 2$).

Assuming anechoic terminations up- and downstream in the Herschel-Quincke arrangement, the system can be tested for stability by studying either of the two nodes. Choosing node A, (see Figure 2), equation (14) still applies with the following definitions of $\boldsymbol{S}$ and $\boldsymbol{R}$ (note that the system now is reduced to a two-port),

$$\boldsymbol{S} = \begin{pmatrix} S^A_{II-II} & S^A_{II-III} \\ S^A_{III-II} & S^A_{III-III} \end{pmatrix}, \tag{17}$$

$$\boldsymbol{R} = \begin{pmatrix} \mathrm{e}^{-\mathrm{i}(k_+ + k_-)L_1} S^B_{I-I} & \mathrm{e}^{-\mathrm{i}(kL_2 + k_- L_1)} S^B_{I-III} \\ \mathrm{e}^{-\mathrm{i}(k_+ L_1 + kL_2)} S^B_{III-I} & \mathrm{e}^{-\mathrm{i}2kL_2} S^B_{III-III} \end{pmatrix},$$

where k is the wave number in duct two and k_+ and k_- are the wave numbers in duct 1 going along with or against the mean flow following the model of Dokumaci [24], including the effects of convection and viscothermal damping but not damping due to turbulence. The latter effect is only important for very low frequencies, which is not relevant here. The elements of the reflection matrix $\boldsymbol{R}$ include the reflections seen at ports A_I and A_{III} from node B (diagonal elements) and the transmission from either port I or III to the other, via node B (off diagonal elements).

4. System characterisation

The scattering matrix (passive part) of the acoustic three-port is determined using the two-microphone wave decomposition technique [25] and applying the source switching method [26]. It is implemented by attaching straight ducts with microphone and loudspeaker arrays to each port of the T-junction, as illustrated in Figure 3. As discussed in the previous section, it is important to ensure that the system is linear when determining the passive properties. Hence, large resistive silencers are attached to each branch to reduce system reflections. The amplitude of the incident sound from the loudspeakers was kept at a moderate level. The mean flow is provided from a pressurized anechoic chamber from which a long, straight duct ($> 60d$) routes the flow to the test rig. Assuming that a fully turbulent flow profile is developed, the mean flow is then monitored by Prandtl tubes. The system is excited using stepped sine in the frequency range 50–2000 Hz. Further details on the setup and instrumentation are found in another paper by the authors [4].

Once the passive part of the system is determined ($\boldsymbol{S}$ and $\boldsymbol{R}$), equation (2) can be rewritten to solve for the source vector as [12]

$$\hat{\boldsymbol{x}}^{s+} = \big(\boldsymbol{E} - \boldsymbol{S}\boldsymbol{R}\big)\big(\boldsymbol{E} + \boldsymbol{R}\big)^{-1} = \boldsymbol{C}\hat{\boldsymbol{x}}. \tag{18}$$

An estimate for the source cross-spectrum matrix $\boldsymbol{G}^s = \hat{\boldsymbol{x}}_2^{s+}\hat{\boldsymbol{x}}_1^{s+*}$ can now be obtained.

However, the direct determination of this matrix involves autospectra at the reference sections in the three ducts, which are sensitive to local turbulence at the microphone positions. The result can be improved using more than one reference cross-section sufficiently separated so that any local turbulence in the measured signals is uncorrelated [12]. The source cross-spectrum estimate then depends only on the cross-spectra between fluctuating quantities. In this work, two reference cross sections are used, yielding

$$\boldsymbol{G}^s = \boldsymbol{T}_+^{-1}\hat{\boldsymbol{x}}_2^{s+}\hat{\boldsymbol{x}}_1^{s+*} = \boldsymbol{T}_+^{-1}\boldsymbol{C}_2\boldsymbol{G}^m\boldsymbol{C}_1^*, \tag{19}$$

where $\boldsymbol{T}$ is the transformation matrix for the source strength vector between the cross-sections, $\boldsymbol{G}_m$ is a 3×3 matrix containing the measured cross-spectra, * is the Hermitian transpose, and the subscripts 1 and 2 denote the two

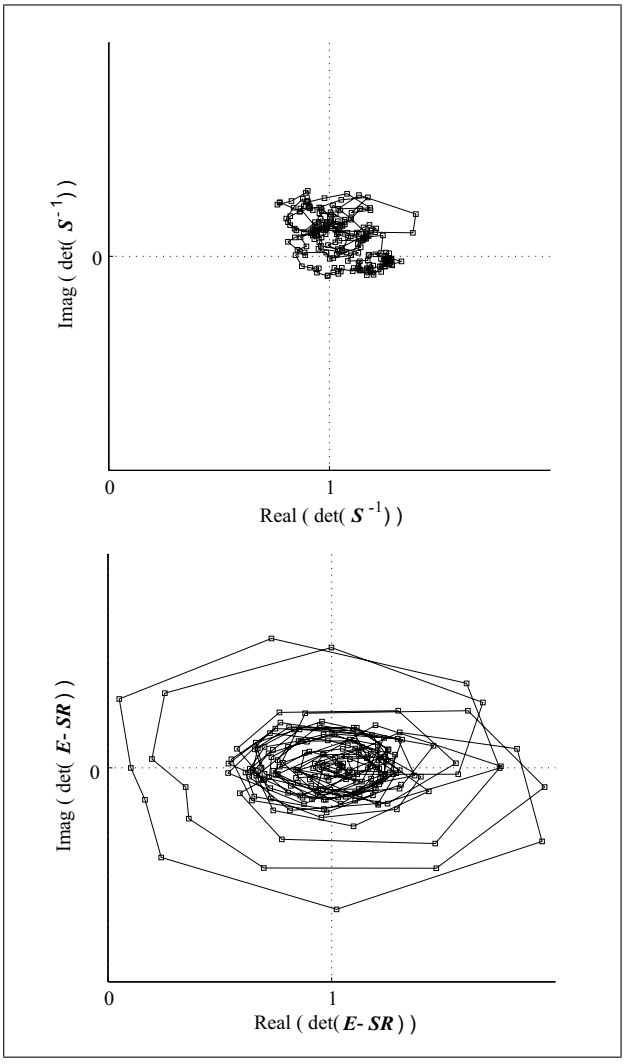

Figure 4. Nyquist stability plot for the T-Junction test rig setup. Top: Check for poles in $\boldsymbol{S}$. Bottom: Check for critical zeros for the complete system according to equation (14). The traces are clockwise with increasing Strouhal number.

reference cross-sections. The diagonal elements of the resulting matrix, $\boldsymbol{G}^s$ represent the autospectra of the source quantity at each port. This procedure compensates for resonance effects in the test rig, and the results relate to the generated noise (outgoing waves with reflection-free terminations) at the three ports.

The quarter wave resonator indicated is not attached when determining the scattering matrix of the T-junction. As described in the previous section, it is only applied to potentially provide the feedback needed for a self-sustained oscillation. The lengths L_3 and L_4 can be varied to tune the system toward different amplification modes of the flow-acoustic interaction.

The experimental validation of the Herschel-Quincke arrangement is made in a similar setup. The mean flow is provided from the same pressurised anechoic chamber used in the previous test. Since no passive measurements are performed here, the loudspeakers are removed – that is, the approaching duct is uninterrupted until the first T-

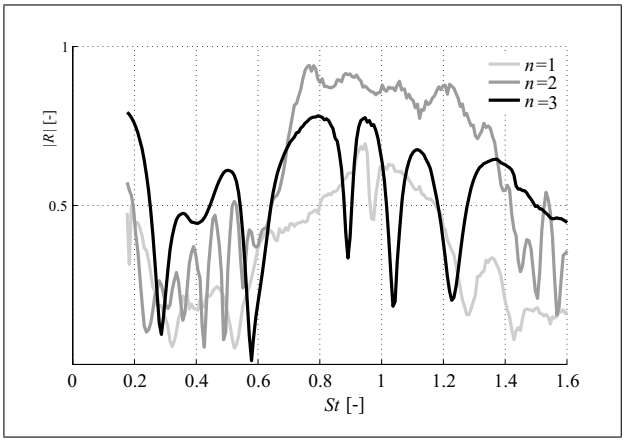

Figure 5. Reflection coefficients given by the test rig terminations as seen at the collapse point of the T-junction (n is the branch index).

Junction. Downstream of the second T-junction, the flow is routed away by a long, straight duct terminated by one of the large resistive silencers used in the previous setup. Microphone pairs are placed up- and downstream of the system as well as in both of the interconnecting ducts. From these microphone pairs, the forward and backward travelling acoustic plane wave amplitudes are calculated.

Today an alternative to experimental determination of the scattering matrix is, as demonstrated in recent papers, numerical methods using LES [14, 27], a linearized Navier Stokes equation approach [28] or an incompressible Navier Stokes solver without turbulence modelling [19].

5. Results

All results are based on the characterisation of a T-junction where the side branch orifice is subjected to grazing flow with a mean Mach number of 0.15. The system has been validated for linearity [4] and can also be shown to be stable by applying equation (14) to the measured data. Figure 4 shows that there are no critical poles in $\boldsymbol{S}$ and that the complete system, including reflections, is stable. The complete system displays numerous encirclements around the base point $(1, 0\mathrm{i})$ given by reflection free terminations, but none of the encirclements encloses the critical point for stability $(0, 0\mathrm{i})$. The two encirclements that spiral into the critical point are just below and above the second amplification region for the T-junction (shown in the next section).

Figure 5 shows the reflection coefficients at the T-junction looking into each of the three branches. This is interesting for two reasons: first, for the stability analysis to be valid, the system terminations must be passive – that is, they must not amplify the incident sound. The reflections coefficients should be less than unity. Second, the actual values of the reflections coefficients are important when studying if a system whistles. The reflection coefficients are below unity over the whole Strouhal number

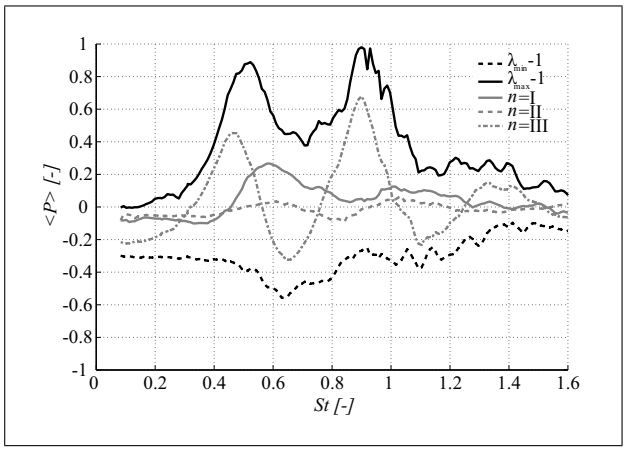

Figure 6. Power balance according to equation (6) and equation (9-10). n indicates Branch number.

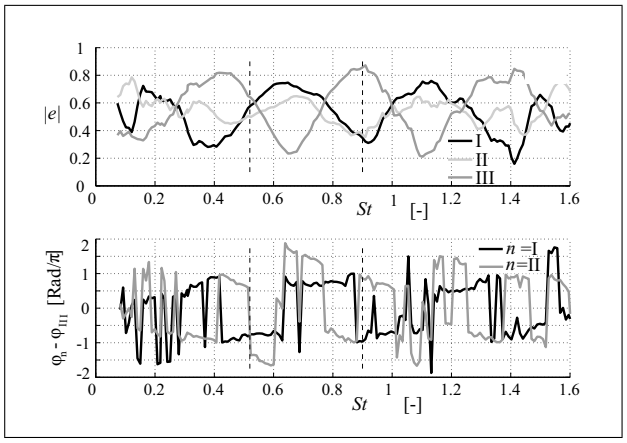

Figure 7. Relative amplitude and phase at the three ports of the incident sound that result in maximum amplification according to equation (9). The vertical dashed lines indicate the maxima of $\lambda_{\max}$.

range studied, but there is a significant difference in the actual values between different Strouhal number ranges. For low Strouhal numbers $St < 0.6$, the reflection coefficients are low, whereas they are considerably higher in the Strouhal number range $0.6 < St < 1.4$. It is shown later that this difference in the reflection coefficients can make a difference in system stability. As discussed in Section 4, only the side branch changes when modifying the system to possibly sustain an oscillation. That is, the reflection coefficients shown here for Branches I and II are also used for the modified setups.

The values of the Strouhal number $St = f d_{\text{eff}}/U$ used here and in the following sections are based on the mean flow velocity and the effective diameter of the duct $d_{\text{eff}} = \pi d/4$.

5.1. Whistling potentiality

Applying the eigenvalue power balance approach equation (9)–(10) to the measured scattering matrix, see Figure 6, shows that there are excitation combinations yielding sound amplification over almost the complete range of Strouhal numbers. There are also distinct peaks where the interaction is strongest. Similarly, there are also excitation combinations that lead to sound attenuation over the whole Strouhal number range. The relative excitation combination of the three ports that yield maximum amplification, $\lambda_{\max}$, can be found by studying the eigenvector from the transformation (see Figure 7). At the second maximum of $\lambda_{\max}$ ($St \sim 0.9$), it is clear that the excitation from the side branch is dominant. This is expected following the explanation model proposed by Nelson *et al.* [29] for the triggering of the flow acoustic interaction. At the first amplification maximum, there is also a noticeable contribution from Branch I. Studying the phase of the incident sound from the up- and downstream ducts relative to the side branch, it seems that it is out of phase with the sound in the side branch when maximum amplification occurs.

The same conclusion can be made (except for the phase information) studying the result for the power balance according to equation (6) in Figure 6. With sound incident from the side branch, n = III, the interactive behaviour of the flow and hydrodynamic fields is clearly indicated: alternating regions with sound amplification and attenuation are visible. Sound incident from Branch I can also result in sound amplification, although the amplification is weaker. In exciting the system from Branch II, the flow-acoustic interaction is generally weak.

Since the resonator arrangement discussed in the previous section would be attached to Branch III, it was decided to tune its resonance frequency to the two first amplification maxima seen in studying equation (6) with n = III. The targeted Strouhal numbers then become 0.45 and 0.9. This corresponds to geometrical lengths $L_3 = 0.34$ or 0.17 m and $L_4 = 0.17$ or 0.085 m for the $St = 0.45$ and 0.90 cases, respectively.

5.2. Whistling

5.2.1. T-junction with side branch resonator

A root-locus type procedure can be used to design the resonators that will provide the required reflection for sustaining an oscillation in the chosen amplification regions. In equation (14) the element in $\boldsymbol{R}$ corresponding to the side branch is varied to see the influence of the reflection in the side branch on the stability of the system. The remaining two elements in $\boldsymbol{R}$ representing the reflections in the up- and downstream duct is left intact since it is only the side branch that is varied in the experimental setup. Studying the frequencies corresponding to the Strouhal numbers at which the resonators are tuned – $St = 0.45$ and 0.90 – a negative real part of the function $D(\omega)$ according to equation (14) may then indicate that the system is unstable. As seen in Figure 8, the system can never become unstable with the resonator tuned to $St = 0.45$ even if the reflection in the side branch is unity. This is because the reflection coefficients in the up- and downstream duct are low in this Strouhal number range (cf. Figure 5). At $St = 0.90$ the system can become unstable if the absolute value of the reflection coefficient is larger than approximately 0.92. This is provided by the resonator arrangement proposed

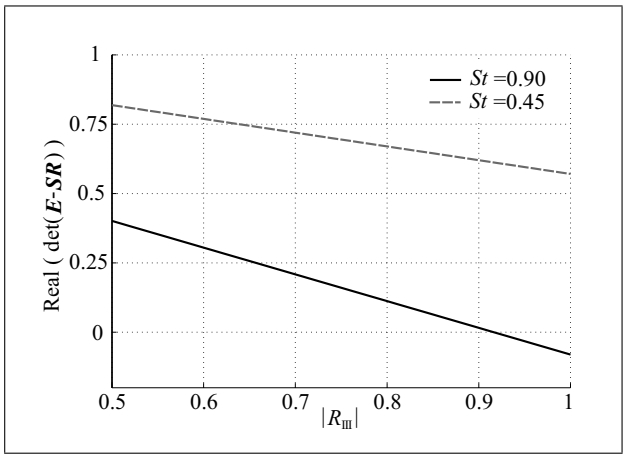

Figure 8. Real part of the function according to equation (14) (at the Strouhal numbers at which the resonators are tuned) as a function of the reflection coefficient in the side branch. A negative value indicates that the system can be unstable.

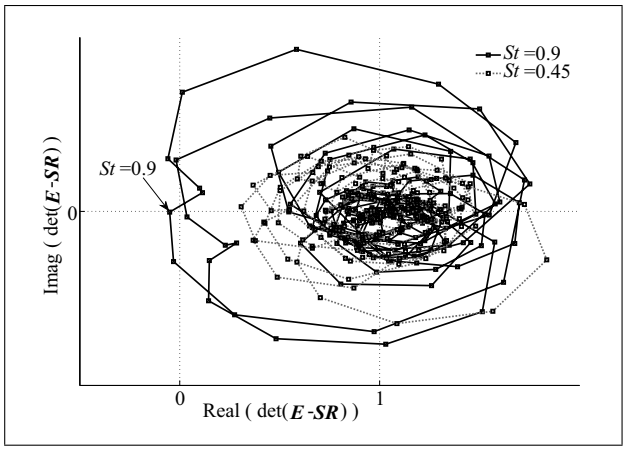

Figure 9. Nyquist stability plot for the T-junction with a resonator arrangement tuned towards $St = 0.45$ and $St = 0.9$. The traces are clockwise with increasing Strouhal number.

in section 4, for which the absolute value of the reflection coefficient is approximately 0.98.

Now applying the stability analysis on the T-junction with the resonator arrangement as described in section 4, it is seen that the configuration tuned to $St = 0.9$ should whistle. The Nyquist plot (Figure 9) displays one encirclement around the critical point (0, 0i) and crossing of the negative real axis at $St = 0.9$. Although not shown here, the same analysis for the same resonator assuming reflection free termination in the up- and downstream duct does not result in an unstable system. Hence, it is not sufficient with excitation from the side branch to actually sustain an oscillation. Reflections from the other ducts are needed as well. As expected, the other resonator arrangement – tuned to $St = 0.45$ – does not make the system unstable.

In Figure 10 the result from the stability analysis is validated experimentally. The normalised oscillation amplitudes of the outward travelling plane waves as given by equation (19) are shown for the up- and downstream duct. As expected, there is a distinct tone for the resonator arrangement tuned to $St = 0.9$, while there is no whistle for the resonator arrangement tuned to $St = 0.45$.

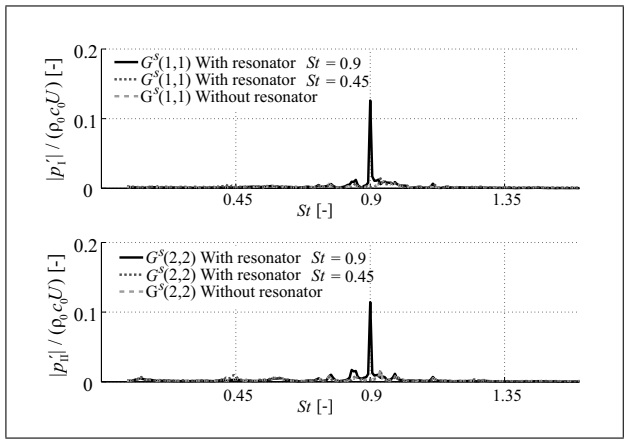

Figure 10. Normalised oscillation amplitudes given by equation (19) with and without resonators.

5.2.2. Herschel-Quincke tube

The length of the straight branch, L_1, is chosen to half the wave length of the frequency corresponding to the first amplification maximum ($St_1 \sim 0.45$, which here yields $L_1 = 0.34$ m) for the T-junction at the given mean flow ($M = 0.15$). Allowing the second branch to be twice the length of duct one yields a system with strong attenuation maxima at odd multiples of St_1. As discussed in section 3, at the even multiples the attenuation of the Herschel-Quincke system is lower. Therefore it is not certain the system can then counteract whistling. Maintaining the length of the main branch L_1 but extending the second branch to three times the length of the first branch, a system with low attenuation at all multiples of St_1 is obtained. Due to practical considerations, the actual lengths of the two ducts in the experimental Herschel-Quincke setup were not exactly as described above. The length of the straight duct segment, L_1, was always 0.335 m while the length of the curved duct, L_2, was 0.62 m or 0.98 m. That is, the actual length ratios were 1.85 and 2.92. For the stability analysis to work satisfactorily, it is important to have a good estimation of these lengths, say within a few percent, since the phase relation in between the amplifying T-junctions is sensitive to the lengths.

Applying the stability analysis according to equation (14) with the modified $\boldsymbol{S}$ and $\boldsymbol{R}$ matrices according to equation (17), the result in Figure 11 is obtained. The arrangement with $L_2/L_1 = 2$ is stable. It may also be noted that the encirclement passing closest to (0, 0i) corresponds to St=0.9 – that is, the first even multiple of St_1. The arrangement with $L_2/L_1 = 3$ should whistle at $St = 0.45$; the other two traces that are close to the critical point are integral multiples of the identified whistle – that is $St = 0.9$ and 1.35. The distance to the origin at the critical frequency is significantly larger here than in the case of the single T-junction with a side branch resonator. The modified $\boldsymbol{S}$ and $\boldsymbol{R}$ matrices used here do not have to be checked for stability separately since they are built from

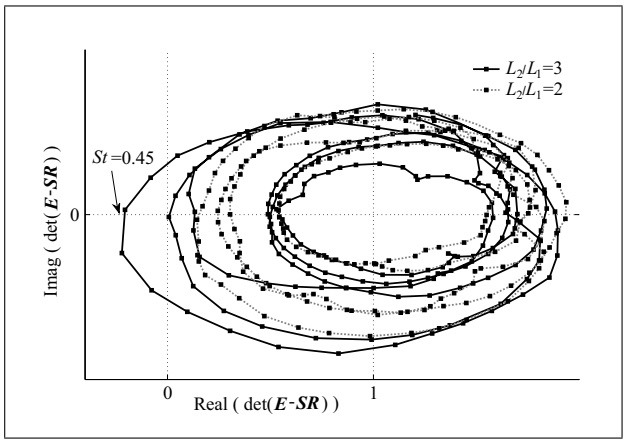

Figure 11. Nyquist stability plot for the two Herschel-Quincke arrangements. The traces are clockwise with increasing Strouhal number.

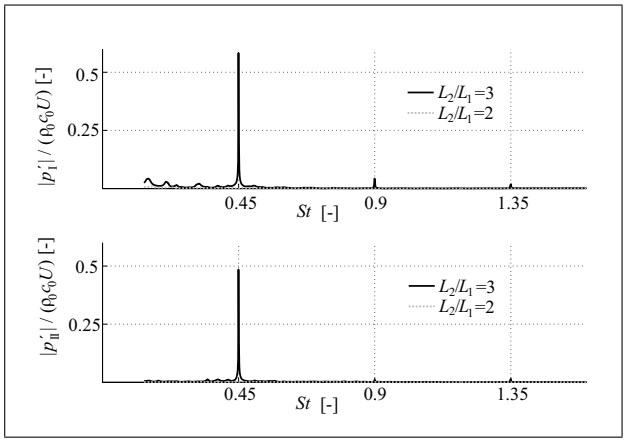

Figure 12. Outward travelling plane wave pressure amplitudes in the up- and downstream direction of the two Herschel-Quincke arrangements.

the elements of the original scattering matrix that has been shown to be stable.

The results are validated in Figure 12. The results presented are the normalized outward travelling plane wave oscillation amplitudes up- and downstream of the Herschel-Quincke tube. For the arrangement with $L_2/L_1 = 3$, as predicted by the stability analysis, a tone is seen at $St = 0.45$. As was indicated by the value of the function $D(\omega)$ at the critical zero crossing, the normalised oscillation amplitude is significantly higher than with the single T-junction with the resonator arrangement. There are also indications of tones at integral multiples of the tone at $St = 0.45$. However, their amplitudes are too low to be self-sustained oscillations. Rather, they are harmonics of the fundamental tone. Finally, also as predicted, the other arrangement of $L_2/L_1 = 2$ does not whistle.

6. Summary and Conclusions

The use of linear multiport models to analyse the existence of flow driven instabilities – that is, self-sustained oscillators or whistles – has been addressed. By combining the scattering and reflection matrices for a system and searching for eigenfrequencies (zeros) in the critical half-plane, the existence of exponentially growing instabilities was determined. Working with experimental data the system behaviour was only known along the positive real axis, and then the search for zeros was made via the so-called Nyquist criterion generalized to an N-DOF system. The method has been validated by two test cases: a T-junction and a Herschel-Quincke tube. In both cases, based on measured data, it was possible to correctly predict whistling that occurred for different configurations. Of course, a linear model cannot predict the level of the resulting oscillations. Also, the exact value of the oscillation frequency can be affected by nonlinear effects. However, as shown by the test cases presented here, the predicted frequencies (based on the Nyquist plot) are in very good agreement with the measured whistling frequencies. There is also support from other investigations – for example, Howe [7] or Martínez-Lera *et al.* [15] – that linear acoustic models of flow driven instabilities are quite accurate in predicting oscillation frequencies. From a practical point of view, the possibility of predicting whistling and of determining the amount of damping needed to avoid such problems is of great importance. In conclusion, one can state that the results presented here are not only of interest from a research perspective, but also have important applications for noise control in pipe and duct systems. It is interesting to note in this context the recent successful attempts to directly compute scattering matrix data [19, 27, 28].

Acknowledgement

The financial support of the Swedish Energy Agency, Project 32022-1, is gratefully acknowledged.

References

[1] P. O. A. L. Davies: Practical flow duct acoustics. Journal of Sound and Vibration **124** (1988) 91–115.

[2] H. Bodén, M. Åbom: Modelling of fluid machines as sources of sound in duct and pipe systems. Acta Acustica **3** (1995) 549–560.

[3] P. Testud, Y. Aurégan, P. Moussou, A. Hirschberg: The whistling potentiality of an orifice in a confined flow using an energetic criterion. Journal of Sound and Vibration **325** (2009) 769–780.

[4] M. Karlsson, M. Åbom: Aeroacoustics of T-junctions – an experimental study. Journal of Sound and Vibration **329** (2010) 1793–1808.

[5] T. Sattelmayer, W. Polifke: Assessment of methods for the computation of the linear stability of combustors. Combustion Science and Technology **175** (2003) 453–476.

[6] T. Sattelmayer, W. Polifke: A novel method for the computation of the linear stability of combustors. Combustion Science and Technology **175** (2003) 477–497.

[7] M. S. Howe: Acoustics of fluid-structure interactions. Cambridge University Press, Cambridge, 1998.

[8] J. M. Rollett: Stability and power-gain invariants of linear twoports. IRE Transactions on circuit theory CT- **9** (1962) 29–32.

[9] M. L. Edwards, J. H. Sinksky: A new criterion for linear 2-port stability using a single geometrically derived para-

meter. IEEE Transactions on Microwave Theory and Techniques **40** (1992) 2303–2311.

[10] H. Nyquist: Regeneration theory. Bell System Technical Journal **11** (1932) 126–147.

[11] N. H. Fletcher, T. D. Rossing: The physics of musical instruments. 2nd ed. Springer Science, New York, 1998.

[12] J. Lavrentjev, M. Åbom: Characterization of fluid machines as acoustic multi-port sources. Journal of Sound and Vibration **197** (1996) 1–16.

[13] Y. Aurégan, R. Starobinski: Determination of acoustical dissipation / production potentiality from the acoustical transfer function of a multiport. Acustica united with Acta Acustica **85** (1999) 788–792.

[14] J. Kopitz, W. Polifke: CFD-based application of the Nyquist criterion to thermo-acoustic instabilities. Journal of Computational Physics **227** (2008) 6754–6778.

[15] P. Martínez-Lera, B. Karthik, C. Schram, S. Föller, R. Kaess, W. Polifke: Low-order modelling of a side branch at low Mach numbers. AIAA 2009-3263, 15th AIAA/CEAS Aeroacoustics Conference, Miami, FL, USA, 2009.

[16] V. Dubos, J. Kergomard, A. Khettabi, J. P. Dalmont, D. H. Keefe, C. J. Nederveen: Theory of sound propagation in a duct with a branched tube using modal decomposition. Acustica united with Acta Acustica **85** (1999) 153–169.

[17] J.-P. Dalmont, C. J. Nederveen, V. Dubos, S. Ollivier, V. Méserette, E. t. Sligte: Experimental determination of the equivalent circuit of an open side hole: Linear and non linear behaviour. Acta Acustica united with Acustica **88** (2002) 567–575.

[18] M. S. Howe: Edge, cavity and aperture tones at very low Mach numbers. Journal of Fluid Mechanics **330** (1997) 61–84.

[19] P. Martínez-Lera, C. Schram, S. Föller, R. Kaess, W. Polifke: Identification of the aeroacoustic response of a low Mach number flow trough a T-joint. Journal of the Acoustical Society of America **126** (2009) 582–586.

[20] G. Kooijman, A. Hirschberg, J. Golliard: Acoustical response of orifices under grazing flow: Effect of boundary layer profile and edge geometry. Journal of Sound and Vibration **315** (2008) 849–874.

[21] J. F. W. Herschel: On the absorption of light by coloured media, viewed in connection with the undulatory theory. Philos. Mag. **3** (1833) 401–412.

[22] G. Quincke: Über Interferenzapparate für Schallwellen (On interference devices for sound waves). Ann. Phys. Chem **128** (1866) 177–192.

[23] M. Karlsson, R. Glav, M. Åbom: The Herschel-Quincke tube: The attenuation conditions and their sensitivity to mean flow. Journal of the Acoustical Society of America **124** (2008) 723–732.

[24] E. Dokumaci: A note on transmission of sound in a wide pipe with mean flow and viscothermal attenuation. Journal of Sound and Vibration **208** (1997) 653–655.

[25] A. F. Seybert, D. F. Ross: Experimental determination of acoustic properties using two-microphone random excitation technique. Journal of the Acoustical Society of America **61** (1977) 1362–1370.

[26] M. L. Munjal, A. G. Doige: Theory of a two source-location method for direct experimental evaluation of the four-pole parameters of an aeroacoustic element. Journal of Sound and Vibration **141** (1990) 323–333.

[27] S. Föller, W. Polifke, D. Tonon: Aeroacoustic characterization of T-junctions based on large eddy simulation and system identification. AIAA-2010-3985, 16th AIAA/CEAS Aeroacoustics Conference, Stockholm, Sweden, 2010.

[28] A. Kierkegaard, S. Boij, G. Efraimsson: A frequency domain linearized navier-stokes equations approach to acoustic propagation in flow ducts with sharp edges. Journal of the Acoustical Society of America **127** (2010) 710–719.

[29] P. A. Nelson, N. A. Halliwell, P. E. Doak: Fluid dynamics of a flow excited resonance. Part II: Flow acoustic interaction. Journal of Sound and Vibration **91** (1983) 375–402.